

Visible light-driven self-heating photocatalytic decarboxylation of fatty acid over $\alpha\text{-Fe}_2\text{O}_3$

Chunlin Hao^{a,c}, Jing Wen^b, Hongxuan Song^b, Bo Huang^b, Guibao Guo^{b,*}, Shengli An^{a,c}

^a Inner Mongolia Key Laboratory of Advanced Ceramic Materials and Devices, School of Materials and Metallurgy, Inner Mongolia University of Science and Technology, Baotou 014010, PR China

^b School of Chemistry and Chemical Engineering, Inner Mongolia University of Science and Technology, Baotou 014010, PR China

^c Key Laboratory of Green Extraction & Efficient Utilization of Light Rare-Earth Resources (Inner Mongolia University of Science and Technology), Ministry of Education, Baotou 014010, PR China



ARTICLE INFO

Keywords:

Photocatalysis

$\alpha\text{-Fe}_2\text{O}_3$

Photothermal conversion effect

Decarboxylation

Boiling solvent

ABSTRACT

Here we report a temperature-dependent strategy that achieves high-efficiency photocatalytic decarboxylation of long-chain fatty acids to C_{n-1} n-alkanes, e.g., producing ~0.5 M of n-heptadecane from stearic acid in a single operation with ~91% selectivity, far beyond no more than mM limit capacities of conventional photocatalysis. Through the use of high boiling-point n-alkane solvents for getting the best self-heating based on the photothermal conversion effect of $\alpha\text{-Fe}_2\text{O}_3$, i.e., high temperatures, which force the standing C-chain at low temperatures down onto the $\alpha\text{-Fe}_2\text{O}_3$ surface for energy-storing, allowing photo-induced hole-electron pairs to readily approach and react with the more strained C-COO⁻ bonds. And the consumption of photogenerated electrons shifts from the conventional PCET of the photo-Koble reaction into a step-wise pathway to form more favorable carbanion intermediate that reacting with H⁺ into RH is accelerated with lifting temperature. Our work offers a practical approach to upgrade photocatalytic decarboxylation by a convenient photo-to-heat route.

1. Introduction

As an sustainable alternative to the fossil fuels, biofuels production from bio-derived fatty acids is a promising pathway for addressing the global energy crisis [1,2]. Currently, the extensively-applied strategy for converting fatty acids into alkanes is hydrodeoxygenation, which is a transition metal-catalyzed process under high temperature and pressure ($\geq 250^\circ\text{C}$, ≥ 2 MPa H₂) [3,4]. The decarboxylation of fatty acids does not consume H₂, and the breaking of the C–C bond requires high temperatures ($\geq 300^\circ\text{C}$), leading to unfavorable cracking and carbon deposition [5,6]. In comparison to the energy-intensive catalytic decarboxylation under high temperature, solar energy-powered photocatalysis enables the transformation of fatty acids into alkanes to take place under mild reaction conditions (room temperature and ambient pressure). In semiconductor photocatalysis, highly active photogenerated holes (h^+) and electrons (e^-) could be generated by photon excitation [7], which has been widely applied in H₂O splitting, CO₂ reduction, and organic synthesis [8–13]. However, there are very limited cases that can reach the scale and efficiency of the existing conventional processes after decades of research. Among many factors, one of the most fatal flaws is the

extremely low quantum efficiency (generally in $\sim 10^{-2}$ level), resulting in the chemical conversion reaction operating in very low concentration (generally in $1\text{--}10^2 \mu\text{M}$). This is ture even for the energetically-downhill decarboxylation reactions [14]. The first report on heterogeneous photocatalytic decarboxylation dates back to 1978, in which Bard and Kraeutler revealed that short-chained fatty acids could be converted to non-polar C_{n-1} alkanes at room temperature on TiO₂ powder by ultra-violet light, and established the photo-Koble reaction, i.e., hole oxidation and conduction electron coupling with proton reduction can be carried out synergistically [15]. However, the resulting alkanes are at trace concentration levels (nM). In 2020, Wang and co-workers utilized the surface hydrogen species from the interactions between additional H₂ ($P(\text{H}_2) \leq 0.2$ MPa) and noble metal-based catalysts (e.g., Pt/TiO₂) to inhibit radical dimerization and oxidation, achieving C_{n-1} alkanes output with $2.25\text{--}3.49 \text{ mmol g}_{\text{cat}}^{-1} \text{ h}^{-1}$ under 365 nm light irradiation [16]. A recent development in photocatalytic decarboxylation of fatty acid is the use of algal enzymes [17–21]. Although the highly-selective alkanes production with AQEs of >80% was achieved by photo-enzymatic decarboxylation of fatty acids under blue light irradiation, their once-through yields are still limited to the 1–30 μM order of

* Corresponding author.

E-mail address: ggb66733@sohu.com (G. Guo).

magnitudes (2 mmol photons $\text{m}^{-2}\text{s}^{-1}$ white light). Moreover, the reaction conditions catalyzed by algal photoenzymes are relatively harsh, requiring relatively high temperature and humidity, which limits the large-scale production of alkanes [22,23]. Such collection of photons to maintain enzyme sustainability rather than simply depending on the excitation of the donor catalyst is reminiscent of the classical photothermal conversion effect, which, if it could help to reverse low AQE and poor single output concentration, would be significant.

The photothermal conversion effect of nanomaterials, resulting from the dissipation of photon energy into heat, has been widely employed for applications in solar energy collection, seawater desalination and cancer therapy [24–29]. Unfortunately, the heat from incident light is rarely used in photocatalysis because its intrinsic driving force is considered to be controlled by the photogenerated charge separation efficiency, with no or negative dependence on the reaction temperature (high temperatures accelerate the h^+/e^- recombination [30]). Only recently, some works focused on the energetically up-hill reactions, reconsidering the influence of heating on heterogeneous photocatalytic redox reaction and h^+/e^- recombination. For instance, in 2023, Zhao's group demonstrated that the photocatalytic hydrogenated dehalogenation of aryl halide with H_2 over In_2O_3 can only be smoothly carried out at 140 °C [31]. In 2023, Mi et al. demonstrated that the solar-to-hydrogen efficiency of photocatalytic H_2O splitting can be greatly improved as the temperature rises from 30 °C to 70 °C [32]. Taking from these examples, it is intuitive that the h_b^+ -initiated and dominated photocatalytic conversion could be accelerated by heating. Specifically, whether the photocatalytic decarboxylation efficiency can be drastically improved and reached a large scale by means of self-heating from the photothermal conversion effect.

In this study, we suggest that self-heating from incident light (410 nm) dramatically enhances the AQE of $\alpha\text{-Fe}_2\text{O}_3$ -based photocatalytic decarboxylation from 0.002% at 98 °C (the boiling point of n-heptane solvent) to 2.38% at 254 °C (the boiling point of n-tetradecane solvent), thereby resulting in a high single output concentration of approximately 0.45 M with a production rate of about 22.4 mmol $\text{g}_{\text{cat}}^{-1}\text{h}^{-1}$. Especially, under concentrated natural solar light ($\sim 20 \text{ W cm}^{-2}$), our large-scale, self-heating photocatalytic stearic acid decarboxylation system (0.05 M, 500 mL) yields n-heptadecane at a rate of approximately 10 mmol $\text{g}_{\text{cat}}^{-1}\text{h}^{-1}$. We demonstrate that heat can bring the standing C-chain at low temperature down onto the $\alpha\text{-Fe}_2\text{O}_3$ surface, endowing greater strain of -C-COOH bond of long-chain fatty acid, which is conducive to photo-induced hole-electron pair approaching and reacting with the energy-storing C-COO⁻ bond.

2. Experiments

2.1. Photocatalytic activity test

The photocatalytic decarboxylation test was carried out under atmospheric pressure following typical procedures: 25 mg of $\alpha\text{-Fe}_2\text{O}_3$ photocatalyst was dispersed into 25 mL solution, which contains 0.05 M of stearic acid, 0.05 M of n-octadecane (internal standard) and n-tetradecane. The mixture was sealed in a homemade quartz photoreactor and degassed with N_2 for 1 hour. The solution was then irradiated by a 410 nm LED array lamp without any external heating. The energy output of the 410 nm LED lamp was 10.25 W cm^{-2} , as measured by an UV energy meter (LS133). A condensing unit keeps the vaporized reaction solution returning to the liquid phase. After illumination, the reaction solution was esterified with methanol and H_2SO_4 (98 wt%) at a constant volume ratio (sample, methanol and H_2SO_4 of 10:10:1) in a silicone oil pan at 85 °C for 2 hours. Finally, the reaction solution from the completed esterification reaction was separated by centrifugation, and the supernatant was collected for GC analysis (GC, Agilent 7820 A; GC-MS, Agilent 7890B-7000 C).

2.2. AQE measurements

The apparent quantum efficiency (AQE) of the visible-light-driven decarboxylation of fatty acids over $\alpha\text{-Fe}_2\text{O}_3$ was determined using a potassium ferrioxalate actinometer with 410 nm LED (10.25 W cm^{-2}) by bottom illumination. The AQE (%) was calculated according to Eq. (1) and the previous report [33].

$$\Phi_c = \frac{k_c \Phi_a}{2.303 k_a \epsilon_{410} L} \times 100\% \quad (1)$$

Where Φ_c is the AQE of $\alpha\text{-Fe}_2\text{O}_3$ -based photocatalytic decarboxylation of fatty acid, k_c is the rate constant (min^{-1}) of visible-light-driven fatty acid decarboxylation, the photolysis quantum yield of $\text{K}_3\text{Fe}(\text{C}_2\text{O}_4)_3$ (Φ_a) at 410 nm is about 1.14 [34], k_a is the rate constant (min^{-1}) of $\text{K}_3\text{Fe}(\text{C}_2\text{O}_4)_3$ under 410 nm LED illumination, ϵ_{410} is the molar absorption coefficient of $\alpha\text{-Fe}_2\text{O}_3$ catalyst at 410 nm and L is the effective optical path of quartz reactor. The detailed calculation process sees the supporting information.

2.3. DFT computational method

The adsorbed stearic acid was established on $\alpha\text{-Fe}_2\text{O}_3$ slab with periodic boundary conditions, including 504 Fe and 756 O atoms in a box of $44 \times 35 \times 37 \text{ \AA}$. A large vacuum layer of 20 \AA was used to avoid the interaction between the two surfaces. First-principles calculations were carried out on the basis of periodic DFT using a generalized gradient approximation within the Perdew-Burke-Ernzerhof exchange correction functional. The adsorption geometry optimization was first conducted with Gamma centered k-point. The wave functions were constructed from the expansion of plane waves with an energy cutoff of 450 eV. The consistence tolerances for the geometry optimization were set as $1.0 \times 10^{-5} \text{ eV/atom}$ for total energy and 0.05 eV/\AA for force, respectively. Subsequently, molecular dynamic (MD) simulations were performed to search stable configurations under different temperatures. The ReaxFF force field was used to simulate the adsorption process. And MD simulations were carried out with a time step of 1.0 fs. The system was first equilibrated for 0.1 ns in an isothermal-isobaric (NVT) ensemble at low temperature and zero pressure, ensuring the minimum energy and internal stress. Finally, the system temperature was raised up to desired 35 and 250 °C. After 100 ps MD simulation, all systems could reach equilibrium state.

3. Results and discussion

3.1. Photocatalytic decarboxylation of stearic acid enabled by photothermal conversion effect

We started our investigation by testing the model reaction of stearic acid decarboxylation with commercially available hematite ($\alpha\text{-Fe}_2\text{O}_3$) nanoparticles as photocatalyst in n-tetradecane solvent under an atmospheric pressure of N_2 under 10.25 W cm^{-2} LED irradiation (410 nm, the wavelength distribution can be found in Fig. S1) without any external heating. $\alpha\text{-Fe}_2\text{O}_3$ is especially attractive as a photocatalyst owing to its abundance, non-toxicity, durability and ability to absorb visible light [35,36]. Characterizations of the $\alpha\text{-Fe}_2\text{O}_3$ catalyst are presented in the Supporting Information (X-ray diffraction patterns see Fig. S2; UV-vis spectra see Fig. S3; BET surface area: 122.4 m^2/g). Photographs of the photocatalytic decarboxylation setup and further details can be found in Fig. 1a and the experimental section. Amazingly, the desired product, n-heptadecane, was obtained in a high yield of 88.4%, with an average production rate of 14.7 mmol $\text{g}_{\text{cat}}^{-1}\text{h}^{-1}$ for the conversion of 0.05 M stearic acid in boiling n-tetradecane solvent (254 °C) over 3 hours of light irradiation (Fig. 1b). Control reactions without a photocatalyst or in darkness offered very little conversion of stearic acid, and yielding less than 2.2% n-heptadecane (Fig. 1b). Consistent

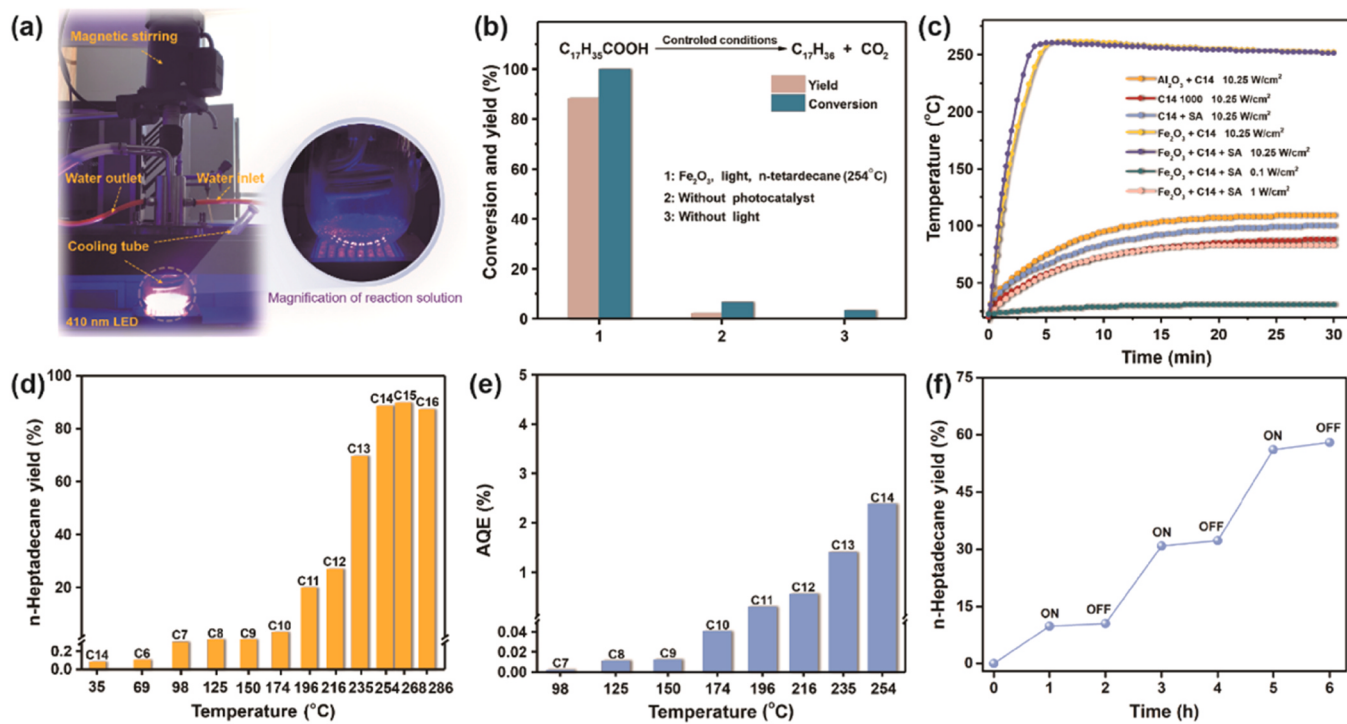


Fig. 1. Photocatalytic performance. (a) Image of self-heated photocatalytic decarboxylation system (lab-scale). (b) Control experiments of stearic acid decarboxylation performance under altered conditions. (c) Monitoring of system temperature under altered conditions. (d) The yields and (e) the AQE of photocatalytic decarboxylation of stearic acid at different temperatures controlled by the n-alkane solvents with different boiling points. General reaction conditions: reaction solution volume (25 mL), α -Fe₂O₃ (25 mg), stearic acid (0.05 M), n-octadecane (internal standard, 0.05 M), atmospheric pressure, boiling n-alkane solvents locked reaction temperature, N₂ atmosphere, LED (410 nm, 10.25 W cm⁻²) irradiation for 3 h. (f) Alternating on and off light experiments for the stearic acid decarboxylation at n-tetradecane solvent-locked temperature (254 °C).

with previous reports [16], the main decarboxylated product was generated through photocatalytic decarboxylation of long-chain fatty acids on Pt/TiO₂ catalysts under specially controlled room-temperature conditions, but the output rate of main product is about 5 folds enhancement. Most strikingly, without any insulation for the photo-reactor, the reaction suspension was rapidly self-heated to the boiling point of n-tetradecane (254 °C) after 3.5 min of 410 nm LED illumination (10.25 W cm⁻²), allowing the reaction to reflux (the reactor was equipped with a condensed water and air-cooled return pipe to return the volatile solution, see Video S1 and Fig. 1c). Apparently, this self-heating is attributed to the photothermal conversion effect of α -Fe₂O₃ nanoparticles, where α -Fe₂O₃ absorbs and converts photons into thermal energy. The photothermal conversion efficiency (η) of α -Fe₂O₃ under 410 nm light illumination is 3.5% (see Support Information for detailed calculations). The solution temperature rises more slowly in the absence of stearic acid, demonstrating that the photocatalytic decarboxylation is an exothermic reaction [14]. However, the n-tetradecane solution temperature with Al₂O₃ powders only reaches approximately 100 °C after 30 minutes of the same light irradiation, which is not significantly different from that of pure n-tetradecane solvent or stearic acid dissolved in n-tetradecane. Moreover, the temperatures of the α -Fe₂O₃/stearic acid/tetradecane suspension enhances with an increase in light intensity, but the temperature rise is negligible under 1 sun of incident light. This phenomenon has historically contributed to the neglect of the semiconductor photothermal conversion effect, especially when the intensity of incident light was intentionally maintained at low levels.

Supplementary material related to this article can be found online at doi:10.1016/j.apcatb.2024.124122.

In general, the rate of photocatalytic reactions depends on the charge separation efficiency and the intensity of the incident light, with little or no dependency on temperature. In some cases, it even shows an inverse

relationship between temperature and reaction rate, as an increase in temperature can lead to charge recombination [30]. Consequently, we initially presumed that heat derived from photothermal conversion would not accelerate our photocatalytic conversion. To test this, we performed an identical reaction in n-tetradecane solvent while controlling the reaction temperature at 35 °C. However, very little conversion of stearic acid and a very low yield of product n-heptadecane (<0.2%) were obtained (Fig. 1d). We then investigated whether the high yield and efficiency observed at 254 °C were due to the temperature or the boiling of the solvent. To explore this, we used a range of n-alkane solvents with varying boiling points (from C₆ n-hexane to C₁₆ n-hexadecane) for the same stearic acid decarboxylation reaction. Notably, all selected n-alkane solvents readily were self-heated to boiling under irradiation, and a dramatic increase in n-heptadecane yield was observed with rising reaction temperature (Fig. 1d). Specifically, from the boiling point of n-hexane (69 °C) to that of n-pentadecane (268 °C), the yield of n-heptadecane increased from 0.1% to 89.6% after 3 hours of light irradiation. This clearly indicates that high temperature, rather than solvent boiling, is responsible for accelerating the decarboxylation of stearic acid. The yield of n-heptadecane did not improve further with temperatures exceeding 268 °C. This is probably ascribed to the fact that the stearic acid substrates and n-heptadecane products are more easily dehydrogenated and cracked at higher temperatures. The apparent quantum efficiency (AQE) of the α -Fe₂O₃-based photocatalytic stearic acid decarboxylation exhibits a remarkable temperature dependence, increasing from 0.002% at the boiling point of n-heptane (98 °C) to 0.238% at the boiling point of n-tetradecane (254 °C) (Fig. 1e). The light/dark experiment with n-tetradecane solvent-locked temperature (254 °C) depicted in Fig. 1f shows that light is essential for this transformation. The blue light/dark experiments, as well as the observed AQE ($\Phi=0.238\%$) for this reaction, rule out a radical chain mechanism. All results suggest that stearic acid decarboxylation is a photocatalytic

process that can be dramatically accelerated by self-heating derived from a certain intensity of light irradiation.

To more comprehensively evaluate the photocatalytic performance, we conducted wavelength-dependent and intensity-dependent experiments. With decreasing wavelength at a constant intensity of 6.8 W cm^{-2} , the yield of n-heptadecane increased (Fig. S4), implying that short-wavelength light is more effective in promoting the decarboxylation of stearic acid. The yield of n-heptadecane was proportional to the power density of the incident light (Fig. S5), indicating that the reaction depends on the number of photons absorbed. We further evaluated various solvents to confirm that self-heating to boiling enhances the yield of photocatalytic stearic acid decarboxylation. As shown in Table 1, under strong light irradiation, all solvents self-heated to boiling, regardless of their polarity. Boiling n-tetradecane was still identified as the optimal solvent. To compare the n-alkanes with high boiling points, the reactions in high boiling point polar solvents or ether compound solvents yielded very low yields of n-heptadecane (Table 1, entries 6, 7, 9, 11). This could be due to competitive adsorption of the solvent on the catalyst, which may hinder the adsorption sites for the stearic acid substrate, impeding subsequent light-induced hole oxidation. Within the same type of solvent, the higher the boiling point, the faster the reaction rate (Table 1, entries 8–11), further demonstrating the temperature-dependent AQE. Other cases such as entries 4, 6 and 7, may result from preferential reactions of the solvent itself with light-induced hole [37]. Kinetic analyses revealed that the photocatalytic decarboxylation of stearic acid at different temperatures follows

first-order reaction kinetics (Fig. S6). The n-heptadecane production rate of $2.0294 \times 10^{-4} \text{ s}^{-1}$ at 254°C is almost 1200 times higher than that at 98°C ($0.0017 \times 10^{-4} \text{ s}^{-1}$) (Fig. S6), further demonstrating the temperature-promoting effect.

3.2. Scope of fatty acids and performances under outdoor sunlight irradiation

To showcase the potential of a temperature-dependent strategy for photocatalytic decarboxylation, we tested a variety of bio-derived long-chain fatty acid substrates. To our delight, all of these fatty acids can be smoothly decarboxylated in boiling long-chain n-tetradecane solvent, giving the corresponding C1-shortened alkanes with good yields (75% ~ 90%) (Table 2, entries 1–10). More surprisingly, in a concentration scale-up reaction with stearic acid at 0.5 M, n-heptadecane was delivered at a very high concentration (~ 0.45 M) in once-through operation with ~ 85% selectivity (Table 2, entry 5). It is worth noting that this output concentration is 5 orders of magnitude higher than those achieved through semiconductor photocatalytic methods or algal photo-enzyme transformations with limited concentrations in the range of $\sim 1\text{--}10^2 \mu\text{M}$ in a single operation. Additionally, the average C_{n-1} n-alkane production rate in our system reaches up to $22.4 \text{ mmol g}_{\text{cat}}^{-1} \text{ h}^{-1}$, which is approximately 10 times or even higher than that of photocatalysis methods or thermocatalysis systems operated under harsh reaction conditions (Table S1). When the concentration scale-up reaction is performed with fatty acid mixtures as substrates, different n-alkane

Table 1
Survey of photocatalytic decarboxylation of stearic acid in different solvents.^a

Entry	Solvent	B.P.T. (°C)	Yield (%)
1		254	88.4
2		98	0.3
3		81	0.4
4		100	<0.1
5		103	0
6		189	2.0
7		203	0.3
8		159	0.5
9		205	2.8
10		142	1.2
11		228	4.6

^a Reaction conditions: the reaction solutions (25 mL) contained stearic acid (0.05 M), n-octadecane (internal standard, 0.05 M), $\alpha\text{-Fe}_2\text{O}_3$ (25 mg) and solvent, atmospheric pressure, N_2 atmosphere, LED irradiation (410 nm, 10.25 W cm^{-2}) with no external heating, 3 h. Boiling point temperature = B. P. T.

Table 2

Visible light-induced self-heating for decarboxylation of fatty acid and fatty acid mixtures on $\alpha\text{-Fe}_2\text{O}_3$.^[a]

R-CH ₂ -COOH	$\alpha\text{-Fe}_2\text{O}_3$, 410nm, N ₂	R-CH ₂ H + CO ₂		
Boiling long-chain n-alkane solvent				
Entry	Substrate	Product	Conv. (%)	Yield (%)
1	CH ₃ (CH ₂) ₂₀ COOH (Behenic acid)	CH ₃ (CH ₂) ₁₉ CH ₃ (n-Heneicosane)	95.4	78.8
2	CH ₃ (CH ₂) ₁₉ COOH (Heneicosanoic acid)	CH ₃ (CH ₂) ₁₈ CH ₃ (n-Nicosane)	98.7	82.5
3	CH ₃ (CH ₂) ₁₈ COOH (Arachidic acid)	CH ₃ (CH ₂) ₁₇ CH ₃ (n-Nonadecane)	91.7	84.7
4	CH ₃ (CH ₂) ₁₇ COOH (Nonadecanoic acid)	CH ₃ (CH ₂) ₁₆ CH ₃ (n-Octadecane)	100.0	79.5
5	CH ₃ (CH ₂) ₁₆ COOH (Stearic acid)	CH ₃ (CH ₂) ₁₅ CH ₃ (n-Heptadecane)	99.9	88.4
6	CH ₃ (CH ₂) ₁₅ COOH (Heptadecanoic acid)	CH ₃ (CH ₂) ₁₄ CH ₃ (n-Hexadecane)	91.2 ^[b]	80.5
7	CH ₃ (CH ₂) ₁₄ COOH (Palmitic acid)	CH ₃ (CH ₂) ₁₃ CH ₃ (n-Pentadecane)	100.0	89.3
8	CH ₃ (CH ₂) ₁₂ COOH (Myristic acid)	CH ₃ (CH ₂) ₁₁ CH ₃ (n-Tridecane)	97.2	85.8
9	CH ₃ (CH ₂) ₁₁ COOH (Tridecanoic acid)	CH ₃ (CH ₂) ₁₀ CH ₃ (n-Dodecane)	98.9	80.7
10	CH ₃ (CH ₂) ₁₀ COOH (Lauric acid)	CH ₃ (CH ₂) ₉ CH ₃ (n-Undecane)	98.4	81.9
11 ^[c]	Stearic acid and palmitic acid (Mol ratio = 1:1)	n-Heptadecane	84.6	61.7
		n-Pentadecane	98.5	84.9
		n-Heptadecane	98.2	80.2

products can be outputted simultaneously with yields exceeding 80% (Table 2, entries 11 and 12), revealing the potential of our strategy for the large-scale production of alkanes from industrial crude fatty acids (obtained through hydrolysis of mixed raw fats). The stability of the $\alpha\text{-Fe}_2\text{O}_3$ catalyst is illustrated in Fig. S7. Under 410 nm illumination (10.25 W cm⁻²), the $\alpha\text{-Fe}_2\text{O}_3$ exhibits no obvious decrease in activity after 5 test cycles (i.e. 10 h irradiation in total), and the crystal structure, optical absorption properties and morphology of the catalyst remain stable during the test. The excellent photoactivity and durability of the $\alpha\text{-Fe}_2\text{O}_3$ catalyst in this photothermal system make it very promising for large-scale applications.

[a] General reaction conditions: the reaction mixture (25 mL) contained substrate (0.05 M), n-octadecane (internal standard, 0.05 M), $\alpha\text{-Fe}_2\text{O}_3$ (25 mg) and n-tetradecane solvent, N₂ atmosphere, LED illumination (410 nm, 10.25 W cm⁻²) with no external heating, 3 h. [b] Concentration-scale reaction with 0.5 M stearic acid, 18 h. [c] Concentration-scale reaction of fatty acid mixtures with stearic acid (0.25 M) and palmitic acid (0.25 M), 18 h.

To further demonstrate the feasibility of our self-heating photocatalytic alkane production strategy, we conducted a scaled-up study (from 0.025 L to 0.5 L, with 0.05 M stearic acid) using outdoor concentrated solar light (about 20 W cm⁻²). A dish light concentrator, featuring a collecting mirror area of about 3.3 m² and equipped with an automatic solar tracking system, replaced artificial light sources to

reduce energy and material costs. Under the concentrated natural solar light irradiation ($\sim 132 \text{ cm}^2$ irradiation area), the reaction solution rapidly self-heated to boiling within 3.5 min (note that no any insulation measures were applied to the reactor, mainly to facilitate observation) (Fig. 2a and Video S2). We observed that the yield of n-heptadecane increased steadily with irradiation time, and the stearic acid could be fully converted into n-heptadecane in $\sim 80\%$ yield during 4 h outdoor test (Fig. 2b). We anticipate that further optimization of the photoreactor, particularly with improved isolation, could significantly reduce the size of the collecting mirror required for the process.

Supplementary material related to this article can be found online at doi:10.1016/j.apcatb.2024.124122.

3.3. Mechanism of self-heating photocatalytic decarboxylation over $\alpha\text{-Fe}_2\text{O}_3$

We then sought to clarify how heat from incident light promotes the photocatalytic decarboxylation reaction. Fig. 3a displays the diffuse reflectance FTIR spectroscopy (DRIFT) of stearic acid adsorbed on $\alpha\text{-Fe}_2\text{O}_3$ at 25 °C. The bands at 1433, 1467, and 1527 cm⁻¹ can be attributed to dissociated stearic acid (C₁₇H₃₅COO_{ad}) [16], and the stearic acid group is bonded on the $\alpha\text{-Fe}_2\text{O}_3$ surface via an O, O' –bidentate coordination bond (1527 cm⁻¹ and 1411 cm⁻¹) at room temperature [38]. Fig. 3b presents the in-situ DRIFT measurement the

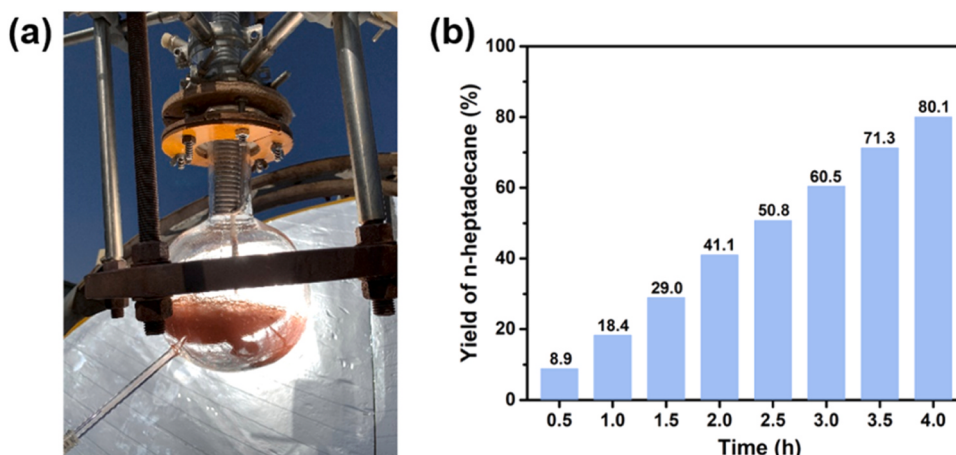


Fig. 2. Practical and large-scale application. (a) Image of outdoor photocatalytic fatty acid decarboxylation scaled-up system under concentrated natural solar light irradiation (about 20 W cm⁻²) in Baotou, China (17/5/2023, 10–25 °C). The diameter of the collecting surface of the dish-shaped concentrator is 2.2 m. (b) The yield of n-heptadecane for the photocatalytic stearic acid decarboxylation in scaled-up volume (500 mL) over $\alpha\text{-Fe}_2\text{O}_3$. Reaction condition: solution volume (500 mL) contained 0.05 M stearic acid, 0.05 M n-octadecane (internal standard), 1 mg/mL $\alpha\text{-Fe}_2\text{O}_3$ and n-tetradecane solvent, atmospheric pressure, N₂.

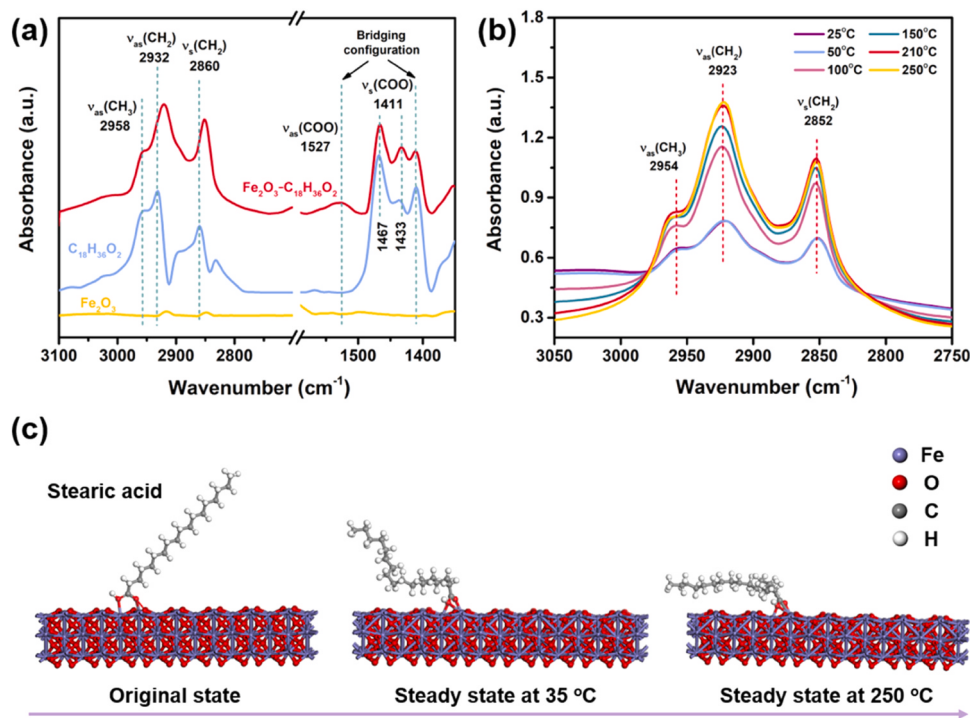


Fig. 3. (a) DRIFT spectra of stearic acid, α -Fe₂O₃ and stearic acid adsorbed on α -Fe₂O₃ surface at room temperature. (b) In situ DRIFT spectra of the stearic acid adsorbed on α -Fe₂O₃ surface in the range of 25–250 °C. (c) Steady state of adsorption models of the stearic acid adsorbed on α -Fe₂O₃ surface at 35 °C and 250 °C from DFT calculations.

adsorption state of stearic acid on the α -Fe₂O₃ surface with programmed temperature increases. As the temperature rises, the signals of the -CH₂- antisymmetric and symmetric stretching vibrations in the nonpolar long-chain moiety of stearic acid at 2923 cm⁻¹ and 2852 cm⁻¹, and the

-CH₃ antisymmetric stretching vibration of the end group at 2954 cm⁻¹, continuously intensify (Fig. 3b). This demonstrates that the fatty chain part of stearic acid gradually attaches to the α -Fe₂O₃ surface propelled by thermal energy. The change in adsorption mode caused by high

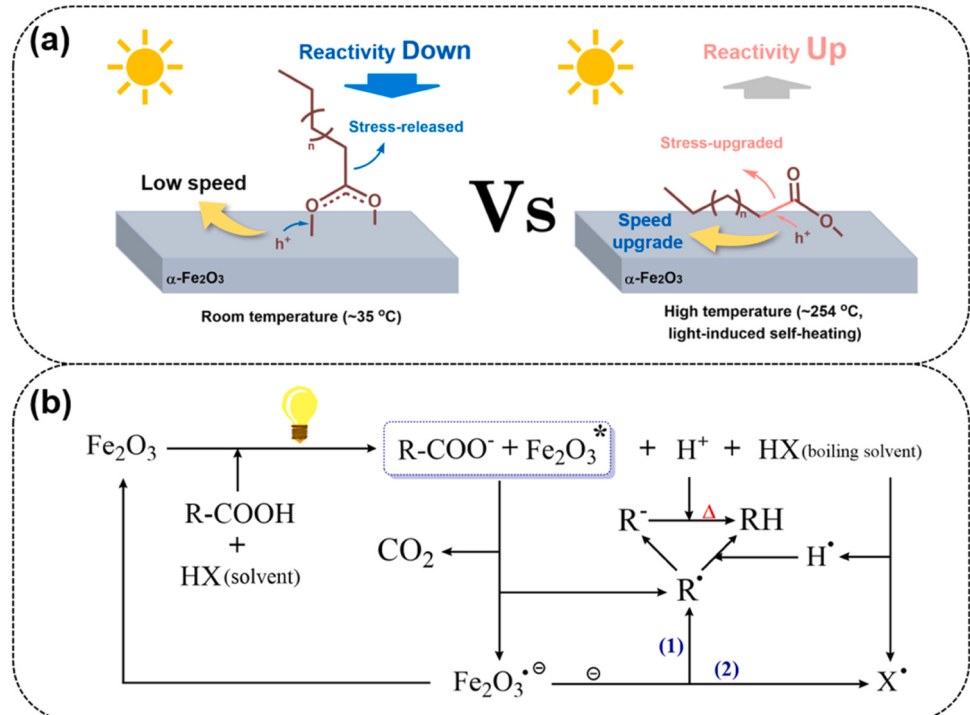


Fig. 4. Schematic illustration of photocatalytic decarboxylation of long-chain fatty acids in boiling long-chain n-alkane solvents over α -Fe₂O₃ catalysts. (a) The long-chain fatty acids accumulate heat energy through shifting to attach to the surface of α -Fe₂O₃ at high temperatures to enable hole activation. (b) Proposed overall reaction pathway. (1) e_{cb} major transfer direction; (2) e_{cb} minor transfer direction.

temperature provides the possibility of high-temperature activation of hole oxidation of stearic acid, namely from an upright to a tilted C-COOH bond (Fig. 4a). It is only under these conditions that h_{vb}^+ -dominated oxidation of the strained C-COOH bond and proton/electron coupling to the tilted C-terminus become more readily achievable than with the upright, non-contact adsorbed C-terminus at low temperatures. However, bending the straight-chain of stearic acid at high temperatures causes greater strain on the C-COOH bond. Such energy storage is highly conducive to the release of CO₂ once hole oxidation commences. The adsorption of stearic acid on the α -Fe₂O₃ surface was simulated through density functional theory (DFT) calculations. Fig. 3c illustrates that stearic acid adsorbs onto the α -Fe₂O₃ surface in the most stable configuration at different temperatures. The results indicate that stearic acid adsorbs on the catalyst surface in an upright configuration at 35 °C, while at 250 °C, the upright configuration on the catalyst surface becomes tilted. The calculated changes in the adsorption model at different temperatures align with the experimental observations.

The enhanced photocatalytic performance is also attributed to the rapid transfer of photoexcited electrons. To explore the potential pathways of light-induced electron transfer, we conducted a series of comparative tests. The results revealed that trace amounts of alkane solvents undergo high-temperature dehydrogenation to produce H₂ and intermediates (Fig. S8). The change in solvent provides a direction for electron transfer [39], which to some extent reduces the accumulation of conduction electrons, thereby accelerating catalytic reaction rates. The capture of electrons by the solvent is verified by the result that the addition of benzaldehyde as electrophile in photocatalytic stearic acid decarboxylation in n-decane solvent gives the desired 1-phenyl-1-undecanol product (Fig. S9). At low boiling temperatures of n-alkane solvents (e.g., n-heptane), the heat is insufficient to break the C-H or C-C bonds (Fig. S8), implying that conduction electrons are not transferred to the solvent at low temperatures. Notably, boiling long-chain n-alkane solvents accelerates the photocatalytic reaction rate by acting as electron sacrificial agents, but this reduction rate is insufficient to match the rate of photo-induced hole oxidation of stearic acid, suggesting that there are other pathways for conduction electron transfer. This will be discussed in detail below.

To determine the hydrogen source of the target product, the deuterated substrate CH₃(CH₂)₁₆COOD was subjected to the reaction, providing the CH₃(CH₂)₁₅CH₂D product with high deuterium incorporation (Fig. S10). This result shows that the hydrogen in the target product mainly stems from the carboxyl hydrogen and minimally from the solvent, from which it can be deduced that the solvent participates in the reaction as a minor process. Consequently, there could be other pathways for the transfer of photogenerated electrons. Radical trapping experiments, where the addition of TEMPO (2,2,6,6-tetramethylpiperidine-1-oxyl) completely quenched the stearic acid decarboxylation reaction (Fig. S11), suggest the existence of C_{n-1} alkyl radical intermediates derived from h^+ -mediated decarboxylation. Previous related studies have shown that the photo-induced electron is transferred via proton-coupled electron transfer (PCET) to react with C_{n-1} alkyl radicals on TiO₂ or Pt/TiO₂ catalysts, thereby affording C_{n-1} alkanes [15,16]. However, the conduction band (CB) potential of α -Fe₂O₃ is insufficient to reduce proton (H⁺/H₂, 0 eV) [40–42]. Previous literature has reported that conduction electrons can be injected into alkyl radicals over homogeneous photocatalysts [43]. Therefore, a direct inference is that alkyl radicals (R·) accept electrons to form alkyl anions (R[−]), which then continue to react with H⁺ to give alkane products in an ionic decarboxylation reaction. To validate this assumption, we introduced benzaldehyde into the lauric acid decarboxylation system, and obtained the overreaction products of 1-phenyl-1-dodecanol, such as 1-phenyl-1-dodecanal and 1-phenyl-1-dodecene (Fig. S12), suggesting the involvement of alkyl anions in the photocatalytic cycle. Moreover, the overreaction products significantly increase with reaction temperature, showing that the reaction between R[−] and H⁺ is temperature-dependent. This is further supported by studies on the

photocatalytic reductive debromination of brominated diphenyl ether (BDE 209) at various temperatures, a classic example of photocatalysis involving carbanion intermediates [44,45]. The results that raising the temperature significantly enhances the degradation of BDE 209 (Fig. S13) confirms that the reaction between carbanion and proton is controlled by thermodynamic collision. These results together manifest that there is a process involving the corresponding anion in the photocatalytic decarboxylation reaction, which is the major pathway for photogenerated electron transfer.

Based on the results and discussion, a plausible mechanism for this catalytic reaction is proposed in Fig. 4 and Fig. S14. Upon strong visible light excitation, α -Fe₂O₃ produces hole-electron (h_{vb}^+/e_{cb}^-) pairs. At low temperature, the photo-induced h_{vb}^+ struggles to approach and react with the C-COO[−] bonds of amphiphilic long-chain fatty acids due to the long fatty chain standing at the interface between the non-polar long-chain n-alkane solvent and the polar α -Fe₂O₃ surface. Consequently, the AQE at room temperature is very low and comparable to that of general photocatalysis. However, elevated temperatures from self-heating induced by incident light enable the standing long-chain of fatty acids at low temperatures to lie flat on the α -Fe₂O₃ surface, facilitating h_{vb}^+ nearby to attack the C-COO[−] bond with more strain. Additionally, with increasing temperature, the reactivity of photo-induced e_{cb}^- changes from the PCET route. Instead, it reacts firstly with R· attached to α -Fe₂O₃ to generate R[−], and then R[−] nucleophilically reacts with H⁺ to produce C_{n-1} n-alkane (R-H) according to the stepwise mechanism. Obviously, the preferential formation of R[−] raised from furthermore conversion of the photo-induced free electron will avoid the h_{vb}^+/e_{cb}^- recombination to a great extent if R[−] intermediate is rapidly consumed away. Since the reaction between R[−] and H⁺ is directly controlled by thermodynamic collisions rather than photo-induced h_{vb}^+/e_{cb}^- , the reaction rate is greatly dependent on temperature. Therefore, combined with the photothermal effect of the α -Fe₂O₃ photocatalyst, the incident light energy can be effectively utilized by increasing the reaction temperature to accelerate the transformation of the substrate.

4. Conclusions

We presented a self-heating photocatalytic decarboxylation on α -Fe₂O₃, with high apparent quantum efficiency, high-flux conversion, and high selectivity towards n-alkanes. The success of this strategy is largely ascribed to the heat originated from the photothermal conversion effect, which enhances the strain of the target C-COO[−] bond by deforming the standing C-chain down at low temperature onto the α -Fe₂O₃ surface, allowing the photo-induced hole-electron pair to initiate the empowered substrate, thereby leading to a huge enhancement in AQE from 0.002% at 98 °C to 2.38% at 254 °C; and the product was generated at a very high concentrations of ~ 0.5 M. This work provides a new idea of using the photo-to-heat effect to substantially improve photocatalytic efficiency to meet the industrial requirements.

CRediT authorship contribution statement

Chunlin Hao: Writing – review & editing, Writing – original draft, Software, Methodology, Investigation, Formal analysis, Data curation. **Jing Wen:** Investigation. **Hongxuan Song:** Investigation. **Shengli An:** Supervision, Resources, Funding acquisition. **Bo Huang:** Investigation. **Guibao Guo:** Supervision, Resources, Methodology, Funding acquisition.

Declaration of Competing Interest

The authors declare that they have no known competing financial interests or personal relationships that could have appeared to influence the work reported in this paper.

Data Availability

Data will be made available on request.

Acknowledgements

This work was financially supported by the National Key R&D Program of China (2020YFC1909105) and the National Natural Science Foundation of China (51974167). We thank Ningbiao Technology Testing Co., Ltd. for providing the DFT calculation.

Appendix A. Supporting information

Supplementary data associated with this article can be found in the online version at [doi:10.1016/j.apcatb.2024.124122](https://doi.org/10.1016/j.apcatb.2024.124122).

References

- [1] E.L. Kunkes, D.A. Simonetti, R.M. West, J.C. Serrano-Ruiz, C.A. Gartner, J. A. Dumesic, Catalytic conversion of biomass to monofunctional hydrocarbons and targeted liquid-fuel classes, *Science* 322 (2008) 417–421.
- [2] N.C. Luo, T. Montini, J. Zhang, P. Fornasiero, E. Fonda, T.T. Hou, W. Nie, J.M. Lu, J.X. Liu, M. Heggen, L. Lin, C.T. Ma, M. Wang, F.T. Fan, S.Y. Jin, F. Wang, Visible-light-driven coproduction of diesel precursors and hydrogen from lignocellulose-derived methylfurans, *Nat. Energy* 4 (2019) 575–584.
- [3] X.Z. Du, X.M. Lei, L.Y. Zhou, Y. Peng, Y. Zeng, H.R. Yang, D. Li, C.W. Hu, H. Garcia, Bimetallic Ni and Mo nitride as an efficient catalyst for hydrodeoxygenation of palmitic acid, *ACS Catal.* 12 (2022) 4333–4343.
- [4] Y. Zeng, H. Wang, H.R. Yang, C. Juan, D. Li, X.D. Wen, F. Zhang, J.J. Zou, C. Peng, C.W. Hu, Ni nanoparticle coupled surface oxygen vacancies for efficient synergistic conversion of palmitic acid into alkanes, *Chin. J. Catal.* 47 (2023) 229–242.
- [5] J. Fu, X.Y. Lu, P.E. Savage, Catalytic hydrothermal deoxygenation of palmitic acid, *Energy Environ. Sci.* 3 (2010) 311–317.
- [6] B. Peng, X. Yuan, C. Zhao, J.A. Lercher, Stabilizing catalytic pathways via redundancy: selective reduction of microalgae oil to alkanes, *J. Am. Chem. Soc.* 134 (2012) 9400–9405.
- [7] G.B. Chen, G.I.N. Waterhouse, R. Shi, J.Q. Zhao, Z.H. Li, L.Z. Wu, C.H. Tung, T. R. Zhang, From solar energy to fuels: Recent advances in light-driven C-I chemistry, *Angew. Chem. Int. Ed.* 58 (2019) 17528–17551.
- [8] P. Zhou, I.A. Navid, Y.J. Ma, Y.X. Xiao, P. Wang, Z.W. Ye, B.W. Zhou, K. Sun, Z. T. Mi, Solar-to-hydrogen efficiency of more than 9% in photocatalytic water splitting, *Nature* 613 (2023) 66–70.
- [9] Y.Z. Zhang, Y.K. Li, X. Xin, Y.J. Wang, P. Guo, R.L. Wang, B.L. Wang, W.J. Huang, A.J. Sobrido, X.H. Li, Internal quantum efficiency higher than 100% achieved by combining doping and quantum effects for photocatalytic overall water splitting, *Nat. Energy* 8 (2023) 504–514.
- [10] X.J. Chen, J. Wang, Y.Q. Chai, Z.J. Zhang, Y.F. Zhu, Efficient photocatalytic overall water splitting induced by the giant internal electric field of a g-C₃N₄/rGO/PDIP Z-scheme heterojunction, *Adv. Mater.* 33 (2021) 2007479.
- [11] M. Bonchio, J. Bonin, O. Ishitani, T.-B. Lu, T. Morikawa, A.J. Morris, E. Reisner, D. Sarkar, F.M. Toma, M. Robert, Best practices for experiments and reporting in photocatalytic CO₂ reduction, *Nat. Catal.* 6 (2023) 657–665.
- [12] W. Song, K.C. Chong, G. Qi, Y. Xiao, G. Chen, B. Li, Y. Tang, X. Zhang, Y. Yao, Z. Lin, Z. Zou, B. Liu, Unraveling the transformation from type-II to Z-scheme in perovskite-based heterostructures for enhanced photocatalytic CO₂ reduction, *J. Am. Chem. Soc.* 146 (2024) 3303–3314.
- [13] Z. Shen, F. Li, L. Guo, X. Zhang, Y. Wang, Y. Wang, X. Jian, X. Gao, Z. Wang, R. Li, C. Fan, J. Liu, Ligand bridged MXene/metal organic frameworks heterojunction for efficient photocatalytic ammonia synthesis, *Appl. Catal. B-Environ. Energy* 346 (2024) 123732.
- [14] Ł. Jęczmionek, K. Porzycka-Semczuk, Hydrodeoxygenation, decarboxylation and decarbonylation reactions while co-processing vegetable oils over a NiMo hydrotreatment catalyst. Part I: thermal effects - theoretical considerations, *Fuel* 131 (2014) 1–5.
- [15] B. Kraeutler, A.J. Bard, Heterogeneous photocatalytic decomposition of saturated carboxylic acids on titanium dioxide powder. Decarboxylative route to alkanes, *J. Am. Chem. Soc.* 100 (1978) 5985–5992.
- [16] Z. Huang, Z. Zhao, C. Zhang, J. Lu, H. Liu, N. Luo, J. Zhang, F. Wang, Enhanced photocatalytic alkane production from fatty acid decarboxylation via inhibition of radical oligomerization, *Nat. Catal.* 3 (2020) 170–178.
- [17] D. Sorigué, B. Légeret, S. Cuiné, S. Blangy, S. Moulin, E. Billon, P. Richaud, S. Brugière, Y. Couté, D. Nurizzo, P. Muller, K. Brettel, D. Pignol, P. Arnoux, Y. Li-Beisson, G. Peltier, F. Beisson, An algal photoenzyme converts fatty acids to hydrocarbons, *Science* 357 (2017) 903–907.
- [18] N.S. Scrutton, Enzymes make light work of hydrocarbon production, *Science* 357 (2017) 872–873.
- [19] M.M.E. Huijbers, W.Y. Zhang, F. Tonin, F. Hollmann, Light-driven enzymatic decarboxylation of fatty acids, *Angew. Chem. Int. Ed.* 57 (2018) 13648–13651.
- [20] F. Li, A. Xia, X. Guo, W. Zhang, Y. Huang, X. Zhu, X. Zhu, Q. Liao, Continuous hydrocarbon fuels production by photoenzymatic decarboxylation of free fatty acids from waste oils, *J. Environ. Chem. Eng.* 11 (2023) 110748.
- [21] X.K. Li, C.G. Page, L. Zanetti-Polzi, A.P. Kalra, D.G. Oblinsky, I. Daidone, T. K. Hyster, G.D. Scholes, Mechanism and dynamics of photodecarboxylation catalyzed by lactate monooxygenase, *J. Am. Chem. Soc.* 145 (2023) 13232–13240.
- [22] S. Hay, N.S. Scrutton, Good vibrations in enzyme-catalysed reactions, *Nat. Chem.* 4 (2012) 161–168.
- [23] G. Bhabha, J. Lee, D.C. Ekiert, J. Gam, I.A. Wilson, H.J. Dyson, S.J. Benkovic, P. E. Wright, A dynamic knockout reveals that conformational fluctuations influence the chemical step of enzyme catalysis, *Science* 332 (2011) 234–238.
- [24] J. Li, Y. Long, X. Cao, H. Sun, R. Jiao, Z. Zhu, W. Liang, A. Li, Recent advances and perspectives in solar photothermal conversion and storage systems: A review, *Adv. Colloid Interfac.* 325 (2024) 103118.
- [25] N.S. Lewis, Research opportunities to advance solar energy utilization, *Science* 351 (2016) 1920.
- [26] W.C. Chueh, C. Falter, M. Abbott, D. Scipio, P. Furler, S.M. Haile, A. Steinfeld, High-flux solar-driven thermochemical dissociation of CO₂ and H₂O using nonstoichiometric ceria, *Science* 330 (2010) 1797–1801.
- [27] J. Wang, Y.Y. Li, L. Deng, N.N. Wei, Y.K. Weng, S. Dong, D.P. Qi, J. Qiu, X.D. Chen, T. Wu, High-performance photothermal conversion of narrow-bandgap Ti₂O₃ nanoparticles, *Adv. Mater.* 29 (2017) 1603730.
- [28] H. Jiang, X. Liu, D. Wang, Z. Qiao, D. Wang, F. Huang, H. Peng, C. Hu, Designing high-efficiency light-to-thermal conversion materials for solar desalination and photothermal catalysis, *J. Energy Chem.* 79 (2023) 581–600.
- [29] R.L. Ge, P.N. Yan, Y. Liu, Z.S. Li, S.Q. Shen, Y. Yu, Recent advances and clinical potential of near infrared photothermal conversion materials for photothermal hepatocellular carcinoma therapy, *Adv. Funct. Mater.* 33 (2023) 2301138.
- [30] P.T.N. Hieu, M. Djavid, K. Cui, Z.T. Mi, Temperature-dependent nonradiative recombination processes in GaN-based nanowire white-light-emitting diodes on silicon, *Nanotechnology* 23 (2012) 194012.
- [31] Z. Wan, C.J. Wang, C. Yang, D.G. Ma, H.W. Ji, C.C. Chen, W.H. Ma, J.C. Zhao, Unusual catalytic hydrogenation caused by photoinduced solid frustrated lewis pairs, *Appl. Catal. B Environ.* 324 (2023) 122237.
- [32] P. Zhou, I.A. Navid, Y.J. Ma, Y.X. Xiao, P. Wang, Z.W. Ye, B.W. Zhou, K. Sun, Z. T. Mi, Solar-to-hydrogen efficiency of more than 9% in photocatalytic water splitting, *Nature* 613 (2023) 66–70.
- [33] P. Zhong, Z.W. Liu, Z.F. Lin, L.R. Kong, Quantum yields study of petroleum hydrocarbons by TiO₂ photodegradation in aquatic solution, *J. Jinan Univ.* 27 (2006) 465–469.
- [34] C.G. Hatchard, C.A. Parker, A new sensitive chemical actinometer 2. Potassium ferrioxalate as a standard chemical actinometer, *Proc. R. Soc. Lond. A* 235 (1956) 518–536.
- [35] Y. Zhao, C. Deng, D. Tang, L. Ding, Y. Zhang, H. Sheng, H. Ji, W. Song, W. Ma, C. Chen, J. Zhao, α -Fe₂O₃ as a versatile and efficient oxygen atom transfer catalyst in combination with H₂O as the oxygen source, *Nat. Catal.* 4 (2021) 684–691.
- [36] O. Zandi, T.W. Hamann, Determination of photoelectrochemical water oxidation intermediates on haematite electrode surfaces using operando infrared spectroscopy, *Nat. Chem.* 8 (2016) 778–783.
- [37] P. Mäki-Arvela, M. Snåre, K. Eränen, J. Myllyoja, D.Y. Murzin, Continuous decarboxylation of lauric acid over Pd/C catalyst, *Fuel* 87 (2008) 3543–3549.
- [38] W. Rachmady, M.A. Vannice, Acetic acid reduction by H₂ over supported Pt catalysts: A DRIFTS and TPD/TPR study, *J. Catal.* 207 (2002) 317–330.
- [39] K. Donabauer, B. König, Strategies for the photocatalytic generation of carbanion equivalents for reductant-free C-C bond formations, *Acc. Chem. Res.* 54 (2021) 242–252.
- [40] C. Pan, M.T. Ou, Q.Z. Cheng, Y. Zhou, Y.K. Yu, Z.M. Li, F. Zhang, D.H. Xia, L. Mei, X.Y. Ji, Z-scheme heterojunction functionalized pyrite nanosheets for modulating tumor microenvironment and strengthening photo/chemodynamic therapeutic effects, *Adv. Funct. Mater.* 30 (2020) 1906466.
- [41] Y.L. Li, Y. Liu, Y.J. Hao, X.J. Wang, R.H. Liu, F.T. Li, Fabrication of core-shell BiVO₄@Fe₂O₃ heterojunctions for realizing photocatalytic hydrogen evolution via conduction band elevation, *Mater. Des.* 187 (2020) 108379.
- [42] M. Ou, C. Pan, Y. Yu, X. Wang, Y. Zhou, H. Zhang, Q. Cheng, M. Wu, X. Ji, L. Mei, Two-dimensional highly oxidized ilmenite nanosheets equipped with Z-scheme heterojunction for regulating tumor microenvironment and enhancing reactive oxygen species generation, *Chem. Eng. J.* 390 (2020) 124524.
- [43] Y. Yoshimi, T. Itou, M. Hatanaka, Decarboxylative reduction of free aliphatic carboxylic acids by photogenerated cation radical, *Chem. Commun.* (2007) 5244–5246.
- [44] W. Peng, Y.H. Lin, Z. Wan, H.W. Ji, W.H. Ma, J.C. Zhao, An unusual dependency on the hole-scavengers in photocatalytic reductions mediated by a titanium-based metal-organic framework, *Catal. Today* 340 (2020) 86–91.
- [45] C.Y. Sun, C.C. Chen, W.H. Ma, J.C. Zhao, Photocatalytic debromination of decabromodiphenyl ether by graphitic carbon nitride, *Sci. China Chem.* 55 (2012) 2532–2536.